ISTITUTO NAZIONALE DI RICERCA METROLOGICA
Repository Istituzionale

Accurate Parameters Identification of a Supercapacitor Three-Branch Model

(Article begins on next page)

05 February 2025

RESEARCH ARTICLE

Accurate Parameters Identification of a Supercapacitor Three-Branch Model

MAURO ZUCCA[1], **(Senior Member, IEEE), MELIKA HASSANZADEH**[1,2],
ORNELLA CONTI[2], **AND UMBERTO POGLIANO**[1]
[1]Istituto Nazionale di Ricerca Metrologica (INRIM), 10135 Turin, Italy
[2]Politecnico di Torino, 10129 Turin, Italy

Corresponding author: Mauro Zucca (m.zucca@inrim.it)

ABSTRACT Supercapacitors are becoming increasingly important storage system components. To effectively control their terminal voltage, even in real time, numerous circuit models capable of faithfully simulating their behavior in energy systems and various applications have been explored. The three-branch supercapacitor model appears to be a good compromise between simplicity and accuracy. Typically, this model lacks accuracy in dynamic cycling and long stand-by periods. In this study, a new model identification method based on the state equations of the circuit is described and tested on a 400 F supercapacitor, and the obtained results are validated by measurements. Such an approach, suitably optimized, provides good agreement with the measurements, with discrepancies below 50 mV even in repeated cycles. In static identification, after 90 minutes of self-discharge, the discrepancy was approximately 5 mV. The study also discusses the sensitivity of the model output to the circuit parameters, which is useful for choosing the appropriate timespan for parameter optimization, and introduces variable leakage resistance and a method for its determination. Using this parameter, good agreement with the measurements is observed during the long self-discharging phases. A discrepancy of less than 50 mV between the measured and computed results is observed after one week. The union of the circuit state equations based model and the nonlinear leakage resistance determination allows the three-branch circuit model to achieve a high accuracy both in real-time simulation and in the presence of long stand-by phases.

INDEX TERMS Analytical modeling, circuit optimization, current measurement, energy storage, resistance, supercapacitors, voltage measurement.

I. INTRODUCTION

Approximately 25 years after their entry into the market, supercapacitors (SCs) have emerged as a pervasive technology. Over the past three decades, the battery energy density has grown significantly, tripling its capacity. SCs have experienced an astonishing 20-fold increase in energy density, reaching up to 100 Wh/kg in the case of hybrid capacitors [1]. With regard to power density, both batteries and SCs undergo a similar, impressive 24-fold increase [1], with SCs exhibiting far superior performance. SCs are a better choice than batteries in high-power density applications with typical charging

The associate editor coordinating the review of this manuscript and approving it for publication was Rui Xiong.

time scales of a few tens of seconds to a few minutes, as well as in low energy density applications and low-temperature environments [2]. The most promising applications are in their integration with batteries, where the SCs provide the required power bursts or cope with quick energy recovery [3], [4], [5], [6], [7], [8], [9], [10], especially in cyclic operations such as braking and accelerating in electric vehicles (EVs). Such applications are numerous to the extent that name them all would take too many rooms. SCs applications range from uninterrupted power supplies (UPSs), cordless screwdrivers, digital cameras to provide flashlights, portable speakers, and hybrid vehicles requiring stop and go driving, including buses, trains, agricultural machinery, excavators, cranes, and forklifts [11]. Other applications include fast

charging for EVs, sensor networks, emergency door operation and eviction slide operation (e.g., in the Airbus A380 jet), emergency power system of More-Electric Aircraft, flexible and wearable SCs, powering in robotics, integrated systems for renewables and energy devices, electric unmanned aerial vehicle applications, and so forth [11], [12], [13], [14].

The use of SCs in real-time applications in electronic circuits requires a circuit model to correctly predict their behavior. For rough sizing in power systems, a linear representation with an RC circuit may be sufficient, especially when integrated into a broader control system [15], [16], [17], [18], [19], [20], [21], [22]. However, this approach is inadequate for designing electronic systems, particularly when the SCs operate intermittently, with longer stand-by periods, for example, when SCs are the storage component in power systems for sensor networks. Manufacturers generally provide only nominal resistance and capacitance but not the parameters of an equivalent circuit model (ECM). As discussed in the next section, there are numerous ECMs and methods for determining their parameters in the literature. However, some require time-consuming procedures that are difficult to implement by designers, others show a lack of accuracy, and in a few studies, it is unclear how to identify some parameters. This study provides a novel identification procedure for a three-branch model based on circuit state equations combined with Conventional Trust Region Reflection (CTRR) optimization. The results are compared with a simple optimization of the approach proposed in [22], which has become a reference in the literature. In addition, this work proposes a novel method to evaluate the leakage resistance behavior as a function of time and voltage, enabling a good correspondence between the model and measurements during prolonged stand-by periods.

II. EQUIVALENT CIRCUIT MODELS IN LITERATURE
Multiple approaches for modeling SCs have been presented in the literature. A comprehensive review of the metrics, mechanisms, and models of SCs can be found in [23], [24], [25], [26], [27], [28], and [29], and electrochemical models, intelligent models, and thermal models are not mentioned here but can be found in the cited papers, for example, [23], [24], [30]. Another alternative to ECMs are the fractional-order models. Using a different mathematical approach, they exhibit good capabilities for fitting experimental data with fewer model parameters. Examples are reported in the literature following the time domain [31], [32], [33], [34], [35] or frequency domain approaches [36], [37].

In the following, the authors would like to recall the main ECMs approaches for reader convenience.

The one branch model is shown in Fig. 1 a), whereas Fig. 1 b) and Fig. 1 c) show a three-stage ladder model [38] and the so-called dynamic model [39], respectively. A comparison between these three models is discussed in [40]. The one-branch model is suitable for a rough design of storage systems but lacks the accuracy required to properly reproduce

the behavior of SCs. Fig. 1 d) shows the two-branch model analyzed in [41] and [42]. In [43], the authors proposed the optimization of a two-branch equivalent circuit that matches the experimental data with a mean relative discrepancy ranging from 0.5 % to 4 %, depending on the current. The transmission line model is a generalization of the three-stage ladder model, as shown in Fig. 1 e). In [26], the authors compared three models: i) the RC model, ii) the two-branch model, and iii) a multi-branch model with respect to the experimental results shown in [44]. The comparison reveals that the multi-branch model better satisfies the experimental results. Fig. 1 f) shows a modified two-branch circuit [45] while Fig. 1 g) is the well-known three-branch Zubieta-Bonert model [22]. Fig. 1 h) represents a combination of configurations 1 f) and 1 g), which is particularly suitable for real-time modeling [46].
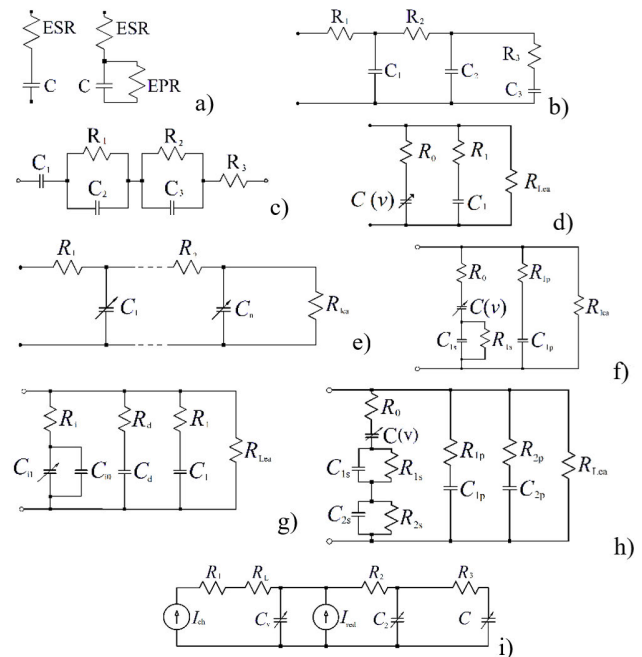

FIGURE 1. Equivalent circuit models of SCs: a) one branch model, b) three-stage ladder model, c) dynamic model, d) two-branch model, e) transmission line model, f) modified two-branch circuit, g) three-branch Zubieta-Bonert model, h) De Carne and colleagues' model, i) Torregrossa and colleagues' model.

Generally, the models are designed to identify the 'trained' SC. A new SC exhibits different behavior than an 'operating' SC, as shown in Fig. 2.

In fact, the charge accumulated in the macropores available at the electrode–electrolyte interface increases with each charge cycle until saturation is reached. Moreover, the charging time, at the same constant current, slightly reduces charging after charging. As shown in Fig. 2, it takes approximately ten charging cycles, or even fewer, to reach saturation [47]. When a SC undergoes a very long stand-by phase or remains unused for a very long time, its behavior resembles that of a non-trained SC. The SC undergoes a relaxation and redistribution phase, resulting in a lower output voltage
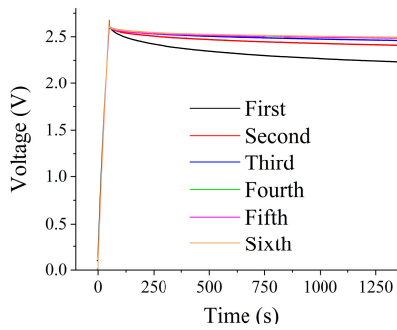
FIGURE 2. 'Training' of a new 400 F supercapacitor to reach a stable output voltage.

during self-discharge compared to a trained capacitor. The model proposed in [47] and shown in Fig. 1 i) incorporates this phenomenon, together with [48], which follows a different approach.

The analysis in this study refers to trained SCs. The model is built for a SC that starts from a known and possibly repeatable condition, and is then controlled over time. Once training has been carried out on the SC, possibly repeated after a long period of relaxation, so that the charge-self-discharge cycle is repeatable, a reference condition is defined. The parameters of the proposed ECM are defined under this condition.

III. MEASUREMENT SETUP

The present study utilizes current and voltage measurements on a SC to identify and verify the proposed models. The current measurement is performed with a LEM IT_65-S Ultrastab transducer, with an expanded uncertainty limited to 0.1 ‰in DC. Two channels of a National Instruments PXI-4461 board fitted with a delta-sigma analog-to-digital converter at 24 bits were used as digitizers. The voltage is measured directly on one channel of the board with a voltage range of ±3.16 V. Measurements are acquired and managed using a program created in the LabVIEW environment. For a long stand-by of a few days or a week, voltage measurements were performed with a reference multimeter (Fluke 8588 A) with an input impedance greater than 10 GΩ and sampling interval of 10 s. The instrumentation was calibrated at INRIM before the measurements. To provide constant charging and discharging current, an ITECH IT-6015-C bidirectional programmable DC power supply is implemented in the experimental setup. All measurements and investigations were performed at a controlled room temperature of 23 ± 0.5°C. The device under test (DUT) is an EDLC Eaton XV series SC with a nominal capacitance of 400 F. The following results are obtained with a charging current of 15 A.

IV. THREE-BRANCH EQUIVALENT CIRCUIT

The three-branch equivalent circuit can provide an excellent simulation of the behavior of SCs with limited complexity. Unlike the two-branch approach, the three-branch circuit allows the simulation of real-time behavior over a long times-

pan. The characteristic of a trained SC, as the one shown in Fig. 2, is the reference for the parameter identification through a charging and self-discharging phenomenological approach. The SC is charged with a constant current i up to the rated voltage (peak). Subsequently, the charging current drops to zero, and the SC undergoes a self-discharging phase, mainly owing to the relaxation and charge redistribution phenomena. The three-branch model proposed in [22] is shown in Fig. 3. Each branch has its own time constant. To simulate nonlinear charging behavior (Fig. 2), a voltage-dependent capacitor is introduced. The first, second, and third branches are called the immediate, delayed, and long-term branches, respectively, based on their time constants.
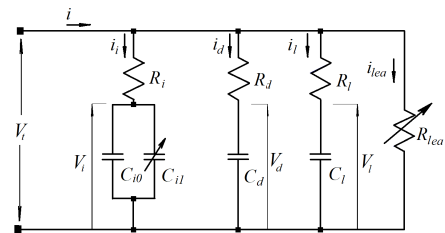

FIGURE 3. 'Three-branch equivalent circuit of a SC.

The first or immediate branch with parameters R_i, C_{i0}, and the voltage-dependent capacitor C_{i1} mainly influences the charging phase within a time range of tens of seconds. The second or delayed branch with parameters R_d and C_d mainly influences the initial part of the discharging phase (usually lasting a few minutes), and the third or long-term branch with parameters R_l, C_l represents the SC behavior in the latter part of the discharging phase, which lasts a few hours. When the three branches reach equilibrium, output voltage V_t no longer changes. To simulate further discharge of the SC, which occurs in the real world, a leakage resistor R_{lea} is added in parallel to the terminal voltage. This qualitative explanation does not properly describe the interdependence between the three branches, as discussed in Section VI-B. For what concern R_{lea}, to the best knowledge of the authors, there are limited references in the literature describing a method to assess this parameter [49]. A novel method is proposed in this study and described in Section V. Furthermore, this involves a significant modification of the equivalent circuit of Fig. 3 with respect to the classic circuit shown in Fig. 1 g), as R_{lea} is no longer a constant resistance but a variable resistance dependent on the voltage.

However, by neglecting R_{lea} as a first approximation, an easy estimation of the other seven circuit parameters in Fig. 3 can be obtained according to [22]. As also verified by other authors (e.g., [47] and [50]), the approach proposed in [22] tends to underestimate the final voltage of the SC in the charging phase; therefore, optimization of the first branch parameters is required to improve accuracy.

A simple and effective optimization can be achieved as follows: the voltage on the first branch capacitors can be

expressed as

$$V_i(t) = \frac{Q_i(t)}{C_i} = \frac{\int_0^t i_i dt}{C_{io} + C_{i1}V_i} = \frac{i_i t}{C_{io} + C_{i1}V_i} \qquad (1)$$

so

$$C_{i1}V_i^2(t) + C_{i0}V_i(t) - i_i t = 0 \qquad (2)$$

where $Q_i(t)$ is the charge stored in the SC versus time and t is the time. The objective function to be minimized is the difference between the measured terminal voltage $V_{t_{meas}}(t)$ and that obtained by the model V_t, as follows:

$$V_t = V_i + R_i i_i \qquad (3)$$

Therefore, by obtaining $V_i(t)$ from (2), where only the positive solution has a physical meaning and substituting in (3), the objective function $f_{obj}(t)$ is defined as

$$f_{obj}(t) = V_{t_{meas}}(t) - \frac{\left(-C_{io} + \sqrt{C_{io}^2 + 4C_{i1}i_i t}\right)}{2C_{i1}} - R_i i_i \qquad (4)$$

Starting from the initial parameters $z_0 = (C_{io}, C_{i1})_0$ identified according to [22], the function $f_{obj}(t)$ is nonlinear. Therefore, a nonlinear minimization approach is required to optimize the vector parameter $z = (C_{io}, C_{i1})$. This can be achieved by solving a nonlinear least-squares problem, where $f_{obj}(t)(z)$ is a vector, with n elements being the function values at each measured time sample $V_{t_{meas}}(t)$. So that:

$$f_{obj}(z) = \begin{bmatrix} f_{obj1}(z) \\ f_{obj2}(z) \\ \vdots \\ f_{objn}(z) \end{bmatrix} \qquad (5)$$

The nonlinear least-squares problem can be solved efficiently in the Matlab™ environment using the 'lsqnonlin' function, according to the command: z = lsqnonlin $(f_{obj}(z), z_0)$. As the output, the function returns the optimized parameters $z_{opt} = (C_{io\_opt}, C_{i1\_opt})$ with a CPU time lower than one second, on a common personal computer.

A comparison between the measured values and those obtained using the optimized model is shown in Fig. 4 a). In the same figure, the results of the one-branch model and model [22] are also shown for completeness. Fig. 4 b) shows the absolute voltage difference between the measured and computed values using the optimized model. The maximum discrepancy of 0.11 V, corresponding to a relative difference of 4 % with respect to the rated voltage, occurs when the voltage peak drop is reached, and is mainly due to a time-shift introduced by the model. Except for this peak error, in most of the considered timespan, the error does not exceed 1.5 % (± 0.04 V). After a few hundred seconds, the error shows an increasing trend with time. Indeed, as underlined by other authors, the model does not seem to be suitable for long stand-by phases of the SC. To overcome this problem, a new high-accuracy modeling approach is proposed

in Section VI-A, along with an improvement in the R_{lea} assessment described in the next section.
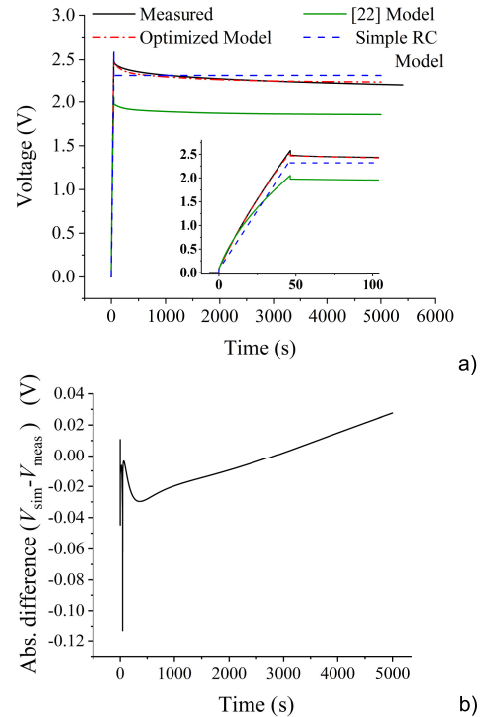

FIGURE 4. a) Comparison between the measured galvanostatic charging and self-discharging for the: i) one-branch model (simple RC), ii) [22] model, and iii) optimized model. b) Absolute difference between the measured voltage and the one computed through the optimized [22] model.

V. LEAKAGE RESISTANCE ASSESSMENT

Following the charging of the SC, once the nominal voltage is reached and the charging current ceases, a self-discharge process occurs, which can be divided into three parts. In the first part, there is a sudden voltage decrease near the peak, lasting a few milliseconds to tens of milliseconds, corresponding to the voltage drop in the internal resistance when the current ceases. Then, in the second part, the voltage decreases owing to the charge redistribution between the three branches of the equivalent circuit, which lasts for approximately a few hours (Fig. 5). Finally, in the long-lasting third part (which can extend for many hours or even days), the voltage decreases owing to the internal electrochemical phenomena. The last part is considered in the model by the leakage resistance R_{lea} which is simply a representation of the phenomenon, even if its physical/chemical nature is likely not only resistive. Indeed, R_{lea} must be a nonlinear parameter to properly mimic the SC behavior under self-discharge. In the model without R_{lea}, the voltage remains constant indefinitely, which is not physically reasonable.

Starting from a discharged SC, we can define the time from the beginning of the SC charging, up to the time where the equilibrium between the internal capacitances is reached, as 'settling time' (ST). This time is approximately 4 hours for
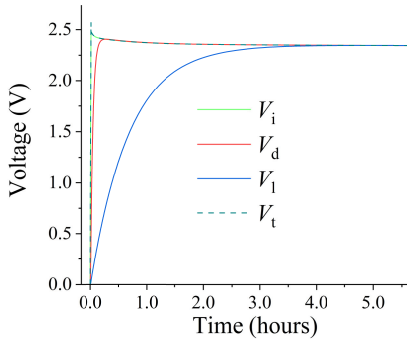
FIGURE 5. Computed behavior of the SC terminal voltage V_t during charging and self-discharging lasting more than 5 hours. The figure shows also the behavior of the voltages of the capacitors C_{i0} and C_{i1} (V_i), C_d (V_d), and C_l (V_l) of the equivalent circuit (Fig. 3). A 400 F SC was considered.

the considered DUT (Fig. 5). For a specific SC, the ST can be verified using the SC model described in Section VI.

To determine R_{lea} for our DUT, we implemented a method that consists of charging the SC up to the rated voltage and then leaving it self-discharging for three days by recording the terminal voltage $V_{t1}(t)$. After three days, the charging and discharging procedure is repeated, and the terminal voltage $V_{t2}(t)$ is measured and recorded for a couple of days by connecting a 10 kΩ auxiliary resistor, R_{aux}, in parallel with the SC. Discharging is quicker as the resistance decreases. A very important point is to connect the auxiliary resistor after approximately twice the ST, because before this time, the effect of the third branch of the equivalent circuit could still be present, which can interfere with the effect of R_{lea}.

R_{aux} can be chosen in order to significantly affect the voltage variation versus time, while avoiding a very quick discharge.

The experimental results are shown in Fig. 6 a). The blue curve represents the discharge of the SC alone (R_{lea}), which is properly fitted by an exponential decay function with three time constants:

$$V_{t1}(t) = V_{01} + a_{11}e^{-\left(\frac{t-t_{11}}{\tau_{11}}\right)} + a_{12}e^{-\left(\frac{t-t_{11}}{\tau_{12}}\right)} + a_{13}e^{-\left(\frac{t-t_{11}}{\tau_{13}}\right)}$$

(6)

where τ_{11}, τ_{12} and τ_{13} are three time constants and V_{01}, a_{11}, a_{12}, a_{13} and t_{11} are the other interpolation parameters.

The green curve represents the discharging of the SC with auxiliary resistance in parallel (R_{lea} // R_{aux}), which is properly fitted with an exponential decay function with two time constants, τ_{21} and τ_{22}.

$$V_{t2}(t) = V_{02} + a_{21}e^{-\left(\frac{t-t_{22}}{\tau_{21}}\right)} + a_{22}e^{-\left(\frac{t-t_{22}}{\tau_{22}}\right)}$$

(7)

and where V_{02}, a_{21}, a_{22} and t_{22} are the other interpolation parameters.

In the model, the equivalent circuit observed by the output resistance R_{lea} is a voltage-dependent capacitance with a small series resistance, which is negligible compared to the output resistance. Therefore, it is reasonable to hypothesize
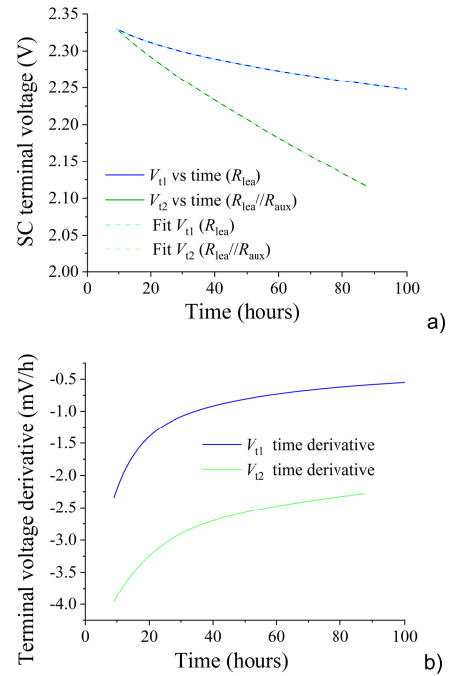

FIGURE 6. a) SC long-term self-discharging behavior. Blue line: self-discharging. Green line: self-discharging with an auxiliary resistor in parallel. b) Time derivatives of the curves in Fig. 6 a).

that the rate of variation of voltage V_t at the terminals of the SC over time depends on the self-discharge current. Without an auxiliary resistor, the self-discharge current can be expressed as

$$\frac{V_{t1}}{R_{lea}(V_{t1})} = C(V_{t1}) \left.\frac{dV_{t1}(t)}{dt}\right|_V$$

(8)

and in presence of the auxiliary resistor, it can be obtained in accordance with

$$\frac{V_{t2}}{\frac{R_{lea}(V_{t2})R_{aux}}{R_{lea}(V_{t2})+R_{aux}}} = C(V_{t2}) \left.\frac{dV_{t2}(t)}{dt}\right|_V$$

(9)

The time behavior of the voltage derivatives is shown in Fig. 6 b). To evaluate the output resistance, (8) and (9) must be considered at the same voltage (i.e., by the horizontal lines in Fig. 6 a)), because in this case, the capacitance seen by the output resistance is the same. The same voltage is obtained at different time instants, where we call t_{lea} the instant at which a specific voltage V_{t1} is obtained with only R_{lea}, and t_{aux} when the same voltage $V_{t2}(t_{aux}) = V_{t1}(t_{lea})$ is obtained in the case *of* R_{lea} // R_{aux}. At the evaluation points, the voltage is the same, and the ratio between (9) and (8) is simplified as

$$R_{lea}(V) = R_{aux}\left[\left.\frac{dV_{t2}(t)}{dt}\right|_{t=t_{aux}} \left(\left.\frac{dV_{t1}(t)}{dt}\right|_{t=t_{lea}}\right)^{-1} - 1\right]$$

(10)

The computed behavior of R_{lea} versus voltage, [$R_{lea} = R_{lea}(V)$] provides a function that increases as the voltage

decreases, as shown in Fig. 7 a) for the considered SC. The trend is well interpolated by a function with two time constants, as shown in (7). Because there is a one-to-one correspondence between the voltage during discharge (blue curve in Fig. 6 a) and time, the R_{lea} time behavior [$R_{lea} = R_{lea}(t)$] can be easily obtained, as shown in Fig. 7 b), which can also be useful in the simulations.
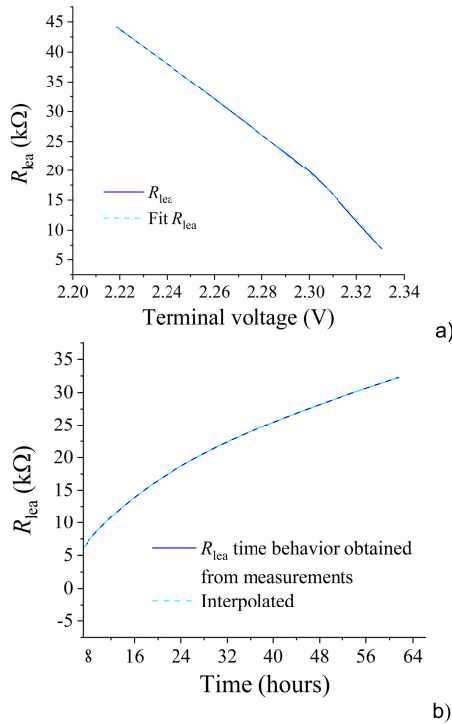

FIGURE 7. Leakage resistance behavior of a 400 F SC a) versus the SC terminal voltage and b) versus time.

The interpolation of Fig. 7 b) can be obtained with a function similar to (7); in particular,

$$R_{lea}(t) = A_0 + A_1 e^{\left(\frac{t}{\tau_1}\right)} + A_2 e^{\left(\frac{t}{\tau_2}\right)} \tag{11}$$

where $R_{lea} = R_{lea}(2 \cdot ST)$ is the initial value of R_{lea} that, for the considered SC, is equal to 6.06 kΩ.

To verify the pattern of R_{lea} in another SC and to verify the variation of the results by changing the R_{aux} we tested a twin SC, same brand and size, with three auxiliary resistors having values of 10 kΩ, 5 kΩ and 1 kΩ to cover at least one order of magnitude variation. The results are shown in Figs. 8 a) and 8 b). The behavior of the R_{lea} versus time is similar to the that of the previous SC with a similar initial value but with a lower resistance increase with time. Fig. 8 a) highlights that by changing the auxiliary resistor, the R_{lea} trend versus time remains the same, but there is a non-constant bias in terms of resistance values at a specific time, which significantly reduces with time. With respect to the determination with $R_{aux} = 10$ kΩ, such a bias determines a variation of the initial R_{lea} up to 37 % for $R_{aux} = 1$ kΩ and approximately 25 % with $R_{aux} = 5$ kΩ, and below 10 % after 36/42 hours (Fig. 8 b).

Such a variation could seem quite high; however, owing to the low sensitivity of the SC terminal voltage with respect to R_{lea} variations (see Section VI-B), this does not compromise the effectiveness of R_{lea} behavior determination, as will be better discussed in Section VI-C.
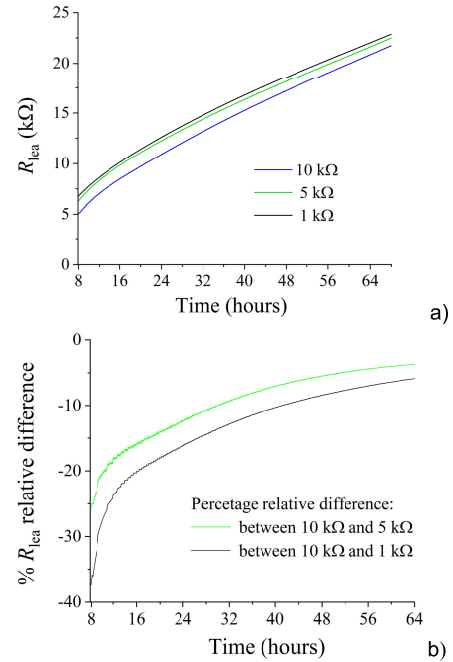

FIGURE 8. a) Leakage resistance vs time with three different R_{aux}, b) resistance percentage relative difference with respect to determination with $R_{aux} = 10$ kΩ.

A useful choice criterion for R_{aux} could be to perform a preliminary measurement, to estimate the initial R_{lea} value and choose a R_{aux} with a resistance value close to that.

VI. OPTIMIZATION BASED ON STATE EQUATIONS
An alternative to the 'classical' identification presented in [22] is proposed below based on the circuit state equations. In this approach, resistance R_{lea} is considered constant to the initial value determined in the previous section.

A. STATE EQUATIONS BASED MODEL
The vector state equation can be obtained with reference to the circuit shown in Fig. 3, as follows:

$$\dot{\boldsymbol{v}} = \boldsymbol{A}\boldsymbol{v} + \boldsymbol{b} \tag{12}$$

where $\boldsymbol{v}$ is the vector representing the state variables, which are the capacitor voltages (13) and $\dot{\boldsymbol{v}}$ is the time-derivative vector (14).

$$\boldsymbol{v} = \begin{bmatrix} V_i \\ V_d \\ V_l \end{bmatrix}; \tag{13}$$

$$\dot{\boldsymbol{v}} = \begin{bmatrix} \frac{dV_i}{dt} \\ \frac{dV_d}{dt} \\ \frac{dV_l}{dt} \end{bmatrix} \tag{14}$$

Equation (12) is nonlinear because the matrix of coefficients A depends on V_i, and b is the control vector.

It is possible to start from Kirchhoff equations at circuit nodes like

$$i_l = i - i_i - i_d \tag{15}$$

and loop equations

$$\begin{cases} V_i - V_d = R_d \cdot i_d - R_i \cdot i_i \\ V_d - V_l = R_l \cdot i_l - R_d \cdot i_d \\ V_l - V_i = R_i \cdot i_i - R_l \cdot i_l \end{cases} \tag{16}$$

by considering that currents are the time derivatives of capacitors charge as:

$$\begin{cases} i_i = \dfrac{dQ_i}{dt} = C_i(V_i) \cdot \dfrac{dV_i}{dt} \\ i_d = \dfrac{dQ_d}{dt} = C_d \cdot \dfrac{dV_d}{dt} \\ i_l = \dfrac{dQ_l}{dt} = C_l \cdot \dfrac{dV_l}{dt} \end{cases} \tag{17}$$

Concerning the first equation in (17) we can better specify that:

$$i_i = \frac{d}{dt}[(C_{i0} + C_{i1}V_i(t))V_i(t)] = C_{io}\frac{dV_i}{dt} + 2C_{i1}V_i\frac{dV_i}{dt}$$

so that $C_i(V_i)$ is:

$$C_1(V_i) = C_{i0} + 2 \cdot C_{i1} \cdot V_i \tag{18}$$

Combining (15) and (16), one can obtain the currents as a function of: the state variables, the resistances, and the total input current i. By substituting the right side of (17) to currents, matrix A and vector b can be easily computed as follows:

$$A = \begin{bmatrix} \dfrac{-(R_d+R_l)}{den \cdot C_1(V_i)} & \dfrac{R_l}{den \cdot C_1(V_i)} & \dfrac{R_d}{den \cdot C_1(V_i)} \\ \dfrac{R_l}{den \cdot C_d} & \dfrac{-(R_l+R_i)}{den \cdot C_d} & \dfrac{R_i}{den \cdot C_d} \\ \dfrac{R_d}{den \cdot C_l} & \dfrac{R_i}{den \cdot C_l} & \dfrac{-(R_i+R_d)}{den \cdot C_l} \end{bmatrix} \tag{19}$$

$$b = \begin{bmatrix} \dfrac{R_d R_l(i-i_{lea})}{den \cdot C_1(V_i)} \\ \dfrac{R_l R_i(i-i_{lea})}{den \cdot C_d} \\ \dfrac{R_i R_d(i-i_{lea})}{den \cdot C_l} \end{bmatrix} \tag{20}$$

where:

$$den = R_i \cdot R_l + R_i \cdot R_d + R_d \cdot R_l \tag{21}$$

When (12) is solved, the SC terminal voltage can be obtained as (21).

$$V_t = \frac{R_d R_l V_i + R_i R_l V_d + R_i R_d V_l + R_i R_d R_l (i - i_{lea})}{den} \tag{22}$$

B. SENSITIVITY ANALYSIS

Starting from the state equations based model, a sensitivity analysis was performed by varying one circuit component value (resistance or capacitance) at a time of $\pm 5\%$ and $\pm 10\%$ with respect to the identified nominal value in the considered DUT. The variations in the SC terminal voltage owing to the variations in the resistance and capacitance values are shown

in Fig. 9. From this analysis, some interesting clues can be deduced regarding the sensitivity of the model output to the circuit parameters and the choice of an appropriate timespan for parameter optimization. Fig. 9 a) shows the variation in the SC terminal voltage V_t owing to the relative variation in the input resistance R_i and clearly shows that the variation in the voltage is associated with the variation in the input current. Fig. 9 b) shows the effect of R_{lea} variations on the terminal voltage. As shown, the variations in R_{lea} affect the output voltage less significantly than other parameters, but its influence increases with time. However, if R_{lea} is not properly chosen or measured and its order of magnitude is incorrect, it can have a significant effect on the identification of the other parameters. Fig. 9 c) and Fig. 9 d) show the variation in the SC terminal voltage owing to the relative variations in C_{i0} and C_{i1}. The sensitivity is very high compared with that of the other parameters. This variation is prevalent during the charging phase of the capacitor. The concavity of the variations for these two parameters is opposed, which is appropriate for optimization. Therefore, from the sensitivity analysis, a suitable timespan for the optimization of these two parameters can be approximately equal to the SC charging time of the equivalent circuit first branch. Fig. 9 e) shows the variation in the SC terminal voltage owing to the relative variations in resistance R_d. In this case, the sensitivity is more than one order of magnitude lower than that of the previous branch, and the effect is maximum after the voltage peak and becomes negligible in approximately half of the settling time.

Fig. 9 f) shows the variation in the SC terminal voltage owing to the relative variations in the resistance C_d. Also in this case, the sensitivity is about one order of magnitude lower than that of the first branch parameters and the effect is maximum in about one third of the settling time and then remains almost constant, with a slow decrease. Fig. 9 g) and Fig. 9 h) show instead the variation of the SC terminal voltage due to the relative variation of the resistance R_l and the capacitance C_l, respectively. Here the initial shape of the graph is similar to those of R_d and C_d, but the time is expanded to about one order of magnitude. The sensitivity is comparable to the other one and, as in the previous case, the sensitivity for the resistance has a sign that is opposed to that of the capacitance.

The different behaviors in time and shape of these graphs, and their similar sensitivities, allow us to consider the optimization of R_d, C_d, R_l and C_l, with a proper choice of the timespan, approximately from the end of the charging of the first branch to the end of the ST of capacitances C_d and C_l (e.g., from 2 minutes to 4 hours in Fig. 5).

C. MODEL IDENTIFICATION

Model identification is performed by comparing the model results and experimental measurements within a timespan that is limited but sufficient to allow each of the three branches to affect the terminal voltage of the SC. In our experiments, we verified that one-third of the ST is sufficient for a good model identification.
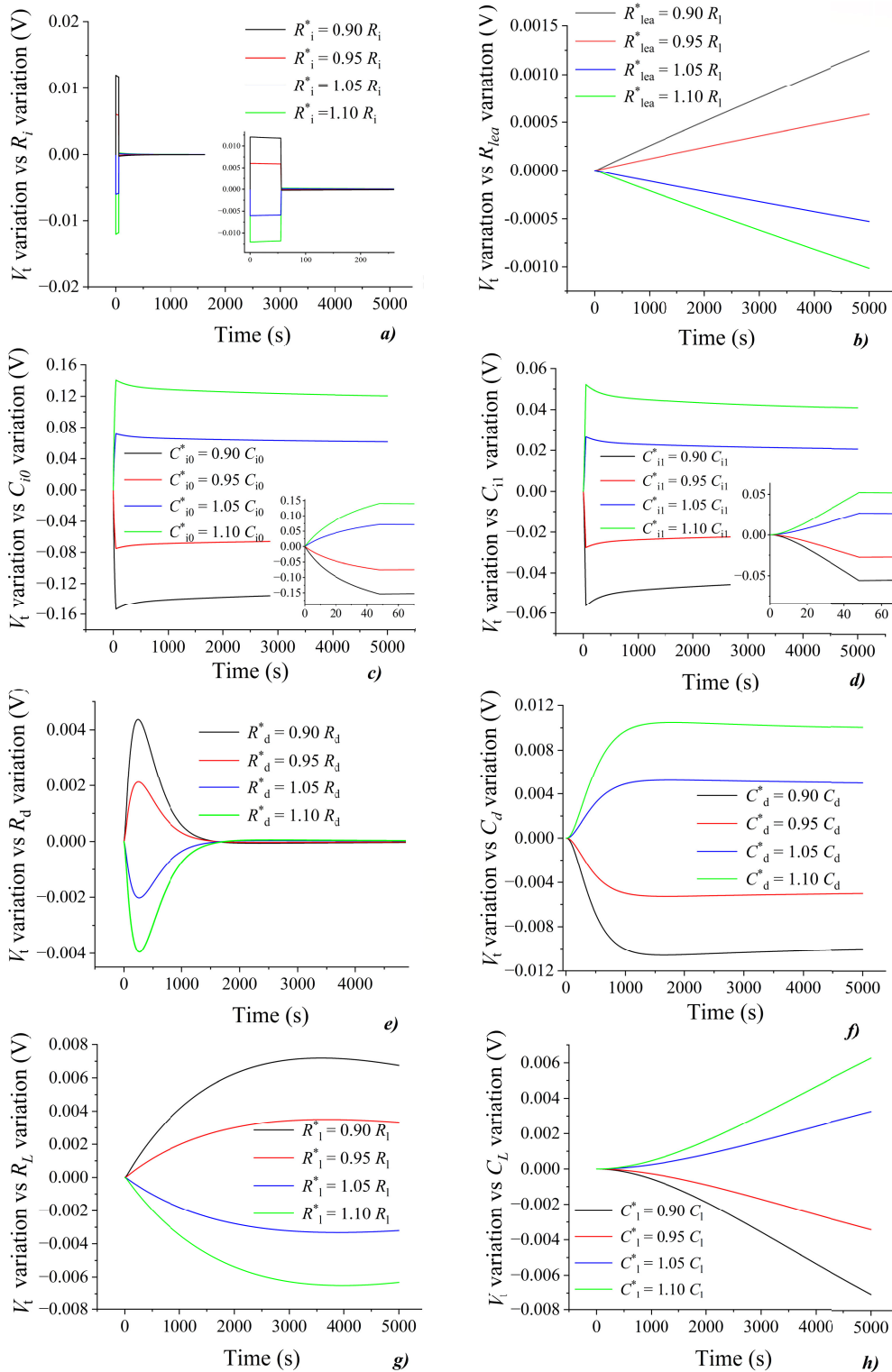
FIGURE 9. Absolute variation ($V_t - V_t^*$) of the SC terminal voltage V_t induced by a variation ± 5 % and ± 10 % of the following parameters: a) R_i, b) R_{lea}, c) C_{i0}, d) C_{i1}, e) R_d, f) C_d, g) R_l, and h) C_l, respectively.

The optimization is obtained using the objective function, which is the difference between two voltages, the one at the terminals of the SC simulated by the model $V_t(t)$ and that measured in the laboratory at the SC terminals $V_{tmeas}(t)$. In addition to the objective function, the optimizer requires some other input data: i) the model equations (matrix A and

vector b), ii) an initial value of the parameters to be identified $(R_d, R_l, C_{i0}, C_{i1}, C_d, C_l)_0$, iii) the initial value of R_{lea} and of the state variables $(V_i, V_d, V_l)_0$, and iv) the value of R_i.

The nonlinear optimizer that we found effective is based on the family of CTRR algorithms [51], [52]. If the optimization algorithm reaches the convergence threshold set by the user, optimized parameters are provided.

A discussion of the optimization algorithm is beyond the scope of this study. Here it is enough to say that there is an efficient tool in Matlab™ for this type of optimization which is the "estimate nonlinear grey-box model parameters" which responds to the command 'nlgreyest' and that can solve the optimization problem summarized in Fig. 10.
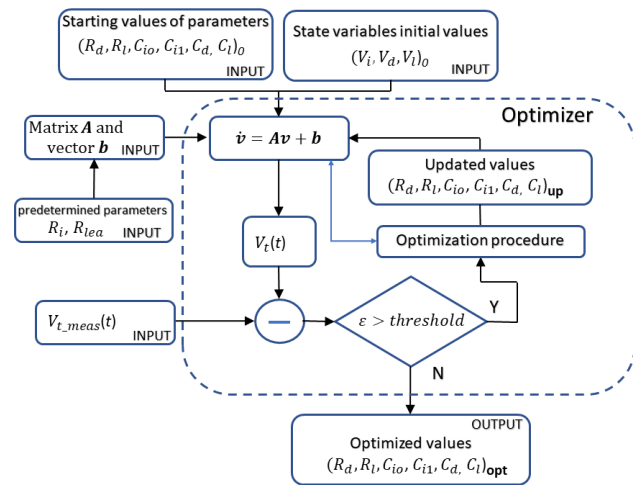
FIGURE 10. Basic scheme of optimization based on state equations. Optimal parameters search is based on CTRR optimization.

Two clarifications regarding the initial parameters, in point ii) above, it is noted that the resistance R_i is missing. R_i is defined as in [22] by the voltage and current (V_1, i_{ch}) at $t_1 = 20$ ms from the starting time in the charging phase of a trained SC, according to

$$R_i = \frac{V_i}{i_{ch}} \quad (23)$$

Regarding the other parameters, it is not necessary to have particularly accurate initial parameters; however, coarse parameters are sufficient for the convergence of the algorithm. Prior identification of the parameters, as in [22], is not necessary. Finally, regarding point iii) mentioned above, for the trained and discharged SC, the initial values of the state variables are equal to zero, and the initial value of R_{lea} must be identified according to Section V.

A point worth of attention is the presence of a bias in the measured current, which is the input for the model, together with the measured voltage at the SC terminals, V_t. Even a very small bias of a few milliamperes, when the current approaches zero, can provide significant variations in the model results.

TABLE 1. 400 F SC equivalent circuit parameters.

R_i (mΩ)	C_{i0} (F)	C_{i1} (F)	R_d (Ω)	C_d (F)	R_l (Ω)	C_l (F)
5.69	261.6	33.05	12.74	11.77	189.1	13.43

VII. SC BEHAVIOR: SIMULATION AND VALIDATION

The state equations based model was used to identify the model of the DUT already considered in Sections IV and V, and its parameters are listed in Table 1.
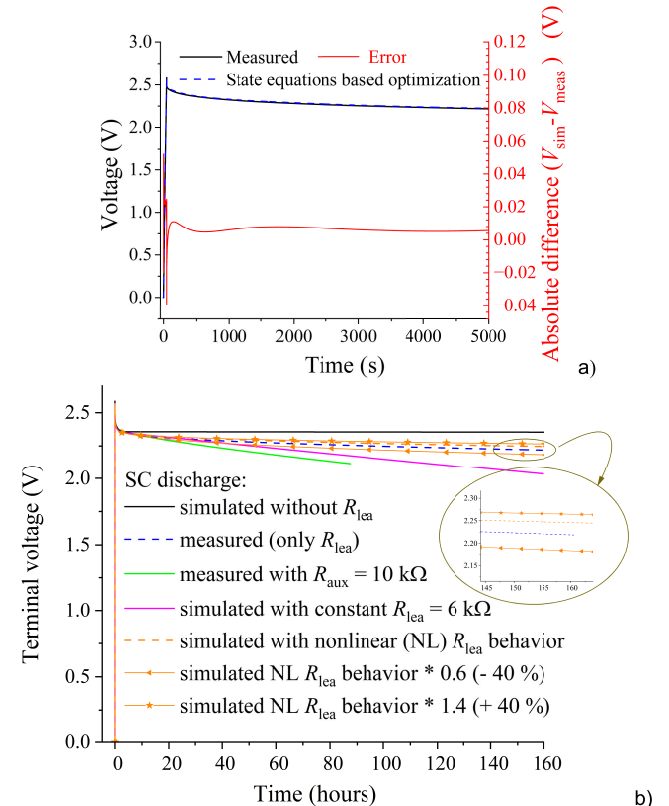

FIGURE 11. Comparison between the voltage measured at the SC terminals and the one computed with the three-branch model identified through the state equations based optimization. The discrepancy ('error') is also shown. a) Static model with constant R_{lea}, b) long-term model with constant and variable R_{lea}.

Fig. 11 a) shows the identification results, where the absolute error, calculated as the difference between the terminal voltage computed by the model and that measured, does not exceed 50 mV around the voltage peak, and then settles to values ten times lower. It should be noted that unlike the identification performed in Section IV (Fig. 4 b), the error does not increase significantly over time. For longer stand-by periods, the previously computed behavior of R_{lea} versus time, as shown in Fig. 7 b), is included in the model. As highlighted in Fig. 11 b), the trend of V_t computed with the nonlinear R_{lea} behavior is very close to the measured one, with discrepancies not exceeding 50 mV. It was pointed out in Section V that the determination of R_{lea} nonlinear behavior is affected by a significant uncertainty and measurements in Section V highlighted variations up to about 40 % in the initial R_{lea} values which are dependent on the choice of the
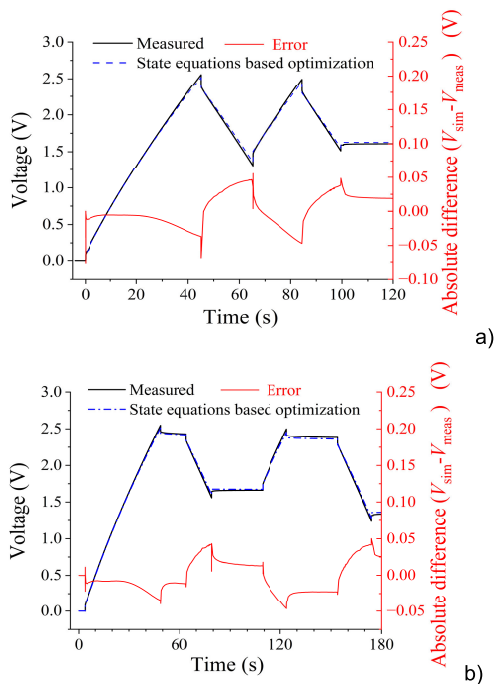
FIGURE 12. Comparison between the SC voltage computed and measured for a) a first sequence and b) a second sequence with stand-by phases. The absolute discrepancies between measured and computed results ('error') are also shown.

R_{aux}. Due to the small sensitivity of the terminal voltage with respect to R_{lea} variations, as highlighted in Fig. 11 b), a variation of $\pm 40\%$ in the R_{lea} nonlinear behavior leads to a discrepancy lower than 50 mV with respect to the measured values ($< 2\%$).

On the contrary, the same diagram highlights that the results obtained with constant R_{lea} clearly show larger discrepancies and are less reliable.

Figs. 12 a) and 12 b) show how, even under dynamic conditions, without (Fig. 12 a) or with (Fig. 12 b) a significant stand-by phase, the absolute error with respect to the measurements remains limited to 50 mV.

VIII. CONCLUSION

This study proposes a method to accurately identify the three-branch equivalent circuit of SCs. In particular, a novel method for determining variable leakage resistance in the SC model is proposed and implemented. The method requires a preliminary determination of the initial values of leakage resistance and internal resistance R_i. The R_{lea} behavior is determined with a measurement procedure that uses an auxiliary resistor. Subsequently, through an optimized approach based on the state equations, other circuit parameters are identified. This approach guarantees a good simulation of the SC behavior for the timespan defined by ST, which is related to the charging time of the third branch. For a longer timespan, basically from twice ST onwards, the nonlinear time behavior of R_{lea} must be measured and implemented in the model. This allows for high accuracy, even for long stand-by phases lasting for several days. The assessment of a nonlinear R_{lea} could also be useful for other ECMs when the

circuit capacitor voltages reach equilibrium, and the further discharge of the device needs to be simulated by the presence of leakage resistance.

REFERENCES
[1] J. Zhao and A. F. Burke, "Review on supercapacitors: Technologies and performance evaluation," *J. Energy Chem.*, vol. 59, pp. 276–291, Aug. 2021, doi: 10.1016/j.jechem.2020.11.013.

[2] N. Kurra and Q. Jiang, "Supercapacitors," in *Storing Energy*. Amsterdam, The Netherlands: Elsevier, Jan. 2022, pp. 383–417.

[3] M. C. Joshi and S. Samanta, "Improved energy management algorithm with time-share-based ultracapacitor charging/discharging for hybrid energy storage system," *IEEE Trans. Ind. Electron.*, vol. 66, no. 8, pp. 6032–6043, Aug. 2019, doi: 10.1109/TIE.2018.2871799.

[4] V. Bolborici, F. P. Dawson, and K. K. Lian, "Hybrid energy storage systems: Connecting batteries in parallel with ultracapacitors for higher power density," *IEEE Ind. Appl. Mag.*, vol. 20, no. 4, pp. 31–40, Jul. 2014, doi: 10.1109/MIAS.2013.2288374.

[5] C. Zhao, H. Yin, and C. Ma, "Equivalent series resistance-based real-time control of battery-ultracapacitor hybrid energy storage systems," *IEEE Trans. Ind. Electron.*, vol. 67, no. 3, pp. 1999–2008, Mar. 2020, doi: 10.1109/TIE.2019.2901640.

[6] A.-A. Mamun, Z. Liu, D. M. Rizzo, and S. Onori, "An integrated design and control optimization framework for hybrid military vehicle using lithium-ion battery and supercapacitor as energy storage devices," *IEEE Trans. Transport. Electrific.*, vol. 5, no. 1, pp. 239–251, Mar. 2019, doi: 10.1109/TTE.2018.2869038.

[7] L. D. Vitan, A. Martin, L. Tutelea, I. Boldea, I. Torac, and N. Muntean, "Supercapacitor city minibus bonded—NdFeB IPMSM propulsion system: Design and system modeling methodology via a case study and laboratory experiments," *IEEE Trans. Ind. Appl.*, vol. 59, no. 2, pp. 1405–1417, Mar. 2023, doi: 10.1109/TIA.2022.3220500.

[8] Q. Xun, Y. Liu, X. Huang, E. A. Grunditz, J. Zhao, and N. Zhao, "Drive cycle energy efficiency of fuel cell/supercapacitor passive hybrid vehicle system," *IEEE Trans. Ind. Appl.*, vol. 57, no. 1, pp. 894–903, Jan. 2021, doi: 10.1109/TIA.2020.3035551.

[9] T. Mesbahi, P. Bartholomeüs, N. Rizoug, R. Sadoun, F. Khenfri, and P. L. Moigne, "Advanced model of hybrid energy storage system integrating lithium-ion battery and supercapacitor for electric vehicle applications," *IEEE Trans. Ind. Electron.*, vol. 68, no. 5, pp. 3962–3972, May 2021, doi: 10.1109/TIE.2020.2984426.

[10] A. Tani, M. B. Camara, and B. Dakyo, "Energy management in the decentralized generation systems based on renewable energy—Ultracapacitors and battery to compensate the wind/load power fluctuations," *IEEE Trans. Ind. Appl.*, vol. 51, no. 2, pp. 1817–1827, Mar. 2015, doi: 10.1109/TIA.2014.2354737.

[11] D. P. Chatterjee and A. K. Nandi, "A review on the recent advances in hybrid supercapacitors," *J. Mater. Chem. A*, vol. 9, no. 29, pp. 15880–15918, 2021.

[12] B. Wang, C. Wang, Z. Wang, S. Ni, Y. Yang, and P. Tian, "Adaptive state of energy evaluation for supercapacitor in emergency power system of more-electric aircraft," *Energy*, vol. 263, Jan. 2023, Art. no. 125632.

[13] A. G. Olabi, Q. Abbas, A. Al Makky, and M. A. Abdelkareem, "Supercapacitors as next generation energy storage devices: Properties and applications," *Energy*, vol. 248, Jun. 2022, Art. no. 123617, doi: 10.1016/j.energy.2022.123617.

[14] C. Xiao, B. Wang, D. Zhao, and C. Wang, "Comprehensive investigation on lithium batteries for electric and hybrid-electric unmanned aerial vehicle applications," *Thermal Sci. Eng. Prog.*, vol. 38, Feb. 2023, Art. no. 101677.

[15] L. Zhang, X. Hu, Z. Wang, F. Sun, J. Deng, and David. G. Dorrell, "Multiobjective optimal sizing of hybrid energy storage system for electric vehicles," *IEEE Trans. Veh. Technol.*, vol. 67, no. 2, pp. 1027–1035, Feb. 2018, doi: 10.1109/TVT.2017.2762368.

[16] M. Passalacqua, D. Lanzarotto, M. Repetto, L. Vaccaro, A. Bonfiglio, and M. Marchesoni, "Fuel economy and EMS for a series hybrid vehicle based on supercapacitor storage," *IEEE Trans. Power Electron.*, vol. 34, no. 10, pp. 9966–9977, Oct. 2019, doi: 10.1109/TPEL.2019.2895209.

[17] S. R. A. Bolonne and D. P. Chandima, "Sizing an energy system for hybrid Li-ion battery-supercapacitor RTG cranes based on state machine energy controller," *IEEE Access*, vol. 7, pp. 71209–71220, 2019, doi: 10.1109/ACCESS.2019.2919345.

[18] E. Schaltz, A. Khaligh, and P. O. Rasmussen, "Influence of battery/ultracapacitor energy-storage sizing on battery lifetime in a fuel cell hybrid electric vehicle," *IEEE Trans. Veh. Technol.*, vol. 58, no. 8, pp. 3882–3891, Oct. 2009, doi: 10.1109/TVT.2009.2027909.

[19] T. Mesbahi, F. Khenfri, N. Rizoug, P. Bartholomeüs, and P. L. Moigne, "Combined optimal sizing and control of Li-ion battery/supercapacitor embedded power supply using hybrid particle Swarm–Nelder–Mead algorithm," *IEEE Trans. Sustain. Energy*, vol. 8, no. 1, pp. 59–73, Jan. 2017, doi: 10.1109/TSTE.2016.2582927.

[20] V. I. Herrera, H. Gaztañaga, A. Milo, A. Saez-de-Ibarra, I. Etxeberria-Otadui, and T. Nieva, "Optimal energy management and sizing of a battery-supercapacitor-based light rail vehicle with a multiobjective approach," *IEEE Trans. Ind. Appl.*, vol. 52, no. 4, pp. 3367–3377, Jul. 2016, doi: 10.1109/TIA.2016.2555790.

[21] A. Kuperman, M. Mellincovsky, C. Lerman, I. Aharon, N. Reichbach, G. Geula, and R. Nakash, "Supercapacitor sizing based on desired power and energy performance," *IEEE Trans. Power Electron.*, vol. 29, no. 10, pp. 5399–5405, Oct. 2014, doi: 10.1109/TPEL.2013.2292674.

[22] L. Zubieta and R. Bonert, "Characterization of double-layer capacitors for power electronics applications," *IEEE Trans. Ind. Appl.*, vol. 36, no. 1, pp. 199–205, Feb. 2000, doi: 10.1109/28.821816.

[23] F. Naseri, S. Karimi, E. Farjah, and E. Schaltz, "Supercapacitor management system: A comprehensive review of modeling, estimation, balancing, and protection techniques," *Renew. Sustain. Energy Rev.*, vol. 155, Mar. 2022, Art. no. 111913, doi: 10.1016/j.rser.2021.111913.

[24] N. Ma, D. Yang, S. Riaz, L. Wang, and K. Wang, "Aging mechanism and models of supercapacitors: A review," *Technologies*, vol. 11, no. 2, p. 38, Mar. 2023, doi: 10.3390/technologies11020038.

[25] S. Zhang and N. Pan, "Supercapacitors performance evaluation," *Adv. Energy Mater.*, vol. 5, no. 6, Mar. 2015, Art. no. 1401401, doi: 10.1002/aenm.201401401.

[26] Z. Cabrane and S. H. Lee, "Electrical and mathematical modeling of supercapacitors: Comparison," *Energies*, vol. 15, no. 3, p. 693, Jan. 2022, doi: 10.3390/en15030693.

[27] A. Berrueta, A. Ursua, I. S. Martín, A. Eftekhari, and P. Sanchis, "Supercapacitors: Electrical characteristics, modeling, applications, and future trends," *IEEE Access*, vol. 7, pp. 50869–50896, 2019, doi: 10.1109/ACCESS.2019.2908558.

[28] H. Miniguano, A. Barrado, C. Fernández, P. Zumel, and A. Lázaro, "A general parameter identification procedure used for the comparative study of supercapacitors models," *Energies*, vol. 12, no. 9, p. 1776, May 2019, doi: 10.3390/en12091776.

[29] L. Zhang, X. Hu, Z. Wang, F. Sun, and D. G. Dorrell, "A review of supercapacitor modeling, estimation, and applications: A control/management perspective," *Renew. Sustain. Energy Rev.*, vol. 81, pp. 1868–1878, Jan. 2018, doi: 10.1016/j.rser.2017.05.283.

[30] Y. Parvini, J. B. Siegel, A. G. Stefanopoulou, and A. Vahidi, "Supercapacitor electrical and thermal modeling, identification, and validation for a wide range of temperature and power applications," *IEEE Trans. Ind. Electron.*, vol. 63, no. 3, pp. 1574–1585, Mar. 2016, doi: 10.1109/TIE.2015.2494868.

[31] T. J. Freeborn, B. Maundy, and A. S. Elwakil, "Measurement of supercapacitor fractional-order model parameters from voltage-excited step response," *IEEE J. Emerg. Sel. Topics Circuits Syst.*, vol. 3, no. 3, pp. 367–376, Sep. 2013, doi: 10.1109/JETCAS.2013.2271433.

[32] L. Zhang, X. Hu, Z. Wang, F. Sun, and D. G. Dorrell, "Fractional-order modeling and state-of-charge estimation for ultracapacitors," *J. Power Sources*, vol. 314, pp. 28–34, May 2016, doi: 10.1016/j.jpowsour.2016.01.066.

[33] R. Prasad, K. Kothari, and U. Mehta, "Flexible fractional supercapacitor model analyzed in time domain," *IEEE Access*, vol. 7, pp. 122626–122633, 2019, doi: 10.1109/ACCESS.2019.2938543.

[34] M. R. Kumar, S. Ghosh, and S. Das, "Charge-discharge energy efficiency analysis of ultracapacitor with fractional-order dynamics using hybrid optimization and its experimental validation," *AEU-Int. J. Electron. Commun.*, vol. 78, pp. 274–280, Aug. 2017, doi: 10.1016/j.aeue.2017.05.011.

[35] Y. Wang, G. Gao, X. Li, and Z. Chen, "A fractional-order model-based state estimation approach for lithium-ion battery and ultra-capacitor hybrid power source system considering load trajectory," *J. Power Sources*, vol. 449, Feb. 2020, Art. no. 227543, doi: 10.1016/j.jpowsour.2019.227543.

[36] N. Bertrand, J. Sabatier, O. Briat, and J.-M. Vinassa, "Embedded fractional nonlinear supercapacitor model and its parametric estimation method," *IEEE Trans. Ind. Electron.*, vol. 57, no. 12, pp. 3991–4000, Dec. 2010, doi: 10.1109/TIE.2010.2076307.

[37] A. Dzielinski, G. Sarwas, and D. Sierociuk, "Comparison and validation of integer and fractional order ultracapacitor models," *Adv. Difference Equ.*, vol. 2011, no. 1, pp. 1–15, Dec. 2011, doi: 10.1186/1687-1847-2011-11.

[38] R. M. Nelms, D. R. Cahela, and B. J. Tatarchuk, "Modeling double-layer capacitor behavior using ladder circuits," *IEEE Trans. Aerosp. Electron. Syst.*, vol. 39, no. 2, pp. 430–438, Apr. 2003, doi: 10.1109/TAES.2003.1207255.

[39] N. Devillers, S. Jemei, M.-C. Péra, D. Bienaimé, and F. Gustin, "Review of characterization methods for supercapacitor modelling," *J. Power Sources*, vol. 246, pp. 596–608, Jan. 2014, doi: 10.1016/j.jpowsour.2013.07.116.

[40] L. Zhang, Z. Wang, X. Hu, F. Sun, and D. G. Dorrell, "A comparative study of equivalent circuit models of ultracapacitors for electric vehicles," *J. Power Sources*, vol. 274, pp. 899–906, Jan. 2015, doi: 10.1016/j.jpowsour.2014.10.170.

[41] D. Xu, L. Zhang, B. Wang, and G. Ma, "Modeling of supercapacitor behavior with an improved two-branch equivalent circuit," *IEEE Access*, vol. 7, pp. 26379–26390, 2019, doi: 10.1109/ACCESS.2019.2901377.

[42] R. Faranda, "A new parameters identification procedure for simplified double layer capacitor two-branch model," *Electric Power Syst. Res.*, vol. 80, no. 4, pp. 363–371, Apr. 2010, doi: 10.1016/j.epsr.2009.10.024.

[43] S. Marín-Coca, A. Ostadrahimi, S. Bifaretti, E. Roibás-Millán, and S. Pindado, "New parameter identification method for supercapacitor model," *IEEE Access*, vol. 11, pp. 21771–21782, 2023, doi: 10.1109/ACCESS.2023.3250965.

[44] F. Belachemi, "Modeling and characterization of electric double-layer supercapacitors used in power electronic," M.S. thesis, Elect. Eng., Inst. Nat. Polytechnique de Lorraine, France, 2000.

[45] V. Musolino, L. Piegari, and E. Tironi, "New full-frequency-range supercapacitor model with easy identification procedure," *IEEE Trans. Ind. Electron.*, vol. 60, no. 1, pp. 112–120, Jan. 2013, doi: 10.1109/TIE.2012.2187412.

[46] G. De Carne, A. Morandi, and S. Karrari, "Supercapacitor modeling for real-time simulation applications," *IEEE J. Emerg. Sel. Topics Ind. Electron.*, vol. 3, no. 3, pp. 509–518, Jul. 2022, doi: 10.1109/JESTIE.2022.3165985.

[47] D. Torregrossa, M. Bahramipanah, E. Namor, R. Cherkaoui, and M. Paolone, "Improvement of dynamic modeling of supercapacitor by residual charge effect estimation," *IEEE Trans. Ind. Electron.*, vol. 61, no. 3, pp. 1345–1354, Mar. 2014, doi: 10.1109/TIE.2013.2259780.

[48] V. Castiglia, N. Campagna, A. O. D. Tommaso, R. Miceli, C. Nevoloso, F. Pellitteri, C. Puccio, and F. Viola, "Modeling, simulation, and characterization of a supercapacitor in automotive applications," *IEEE Trans. Ind. Appl.*, vol. 58, no. 2, pp. 2421–2429, Mar. 2022, doi: 10.1109/TIA.2022.3142707.

[49] H. Yang and Y. Zhang, "Self-discharge analysis and characterization of supercapacitors for environmentally powered wireless sensor network applications," *J. Power Sources*, vol. 196, no. 20, pp. 8866–8873, Oct. 2011.

[50] K. Liu, C. Zhu, R. Lu, and C. C. Chan, "Improved study of temperature dependence equivalent circuit model for supercapacitors," *IEEE Trans. Plasma Sci.*, vol. 41, no. 5, pp. 1267–1271, May 2013, doi: 10.1109/TPS.2013.2251363.

[51] A. R. Conn, N. I. M. Gould, and P. L. Toint, *Trust Region Methods* (MOS-SIAM Series on Optimization), vol. 1. Philadelphia, PA, USA: Society for Industrial and Applied Mathematics, 2000.

[52] R. Prasad, U. Mehta, K. Kothari, M. Cirrincione, and A. Mohammadi, "Supercapacitor parameter identification using grey wolf optimization and its comparison to conventional trust region reflection optimization," in *Proc. Int. Aegean Conf. Electr. Mach. Power Electron. (ACEMP) Int. Conf. Optim. Electr. Electron. Equip. (OPTIM)*, Aug. 2019, pp. 563–569, doi: 10.1109/ACEMP-OPTIM44294.2019.9007158.

MAURO ZUCCA (Senior Member, IEEE) received the degree and the Ph.D. degree in electrical engineering from Politecnico di Torino, in 1994 and 1998, respectively. He achieved the qualification as an Associate University Professor of electrical engineering, in 2012. Since 2017, he has been a Senior Researcher. He is currently the Chief of the ''Electromagnetic Fields and Systems'' Group, INRIM. His impact H-index is 17, according to Scopus. He participated in over 100 conferences, ten of which by invitation, and is the author of about 90 publications in peer-reviewed journals. He was responsible for eight research contracts, participated in 15 research projects: three of them as a Principal Investigator. He is co-author of three patents and a commercial software for computational electromagnetics. His research interests include electrical metrology, study of electromagnetic devices, storage, shielding of power systems, and WPT. He is a member of the Technical Committee TC106, Italian Electrotechnical Committee (CEI), and the Steering Committee of the European Metrology Network for Smart Electricity Grids (EMN-SEG).

MELIKA HASSANZADEH received the B.S. and M.Sc. degrees in electrical engineering from the Babol Noshirvani University of Technology, Babol, Iran, in 2011 and 2014, respectively. She is currently pursuing the Ph.D. degree in metrology with Politecnico di Torino, Italy. She is performing her activity research with INRIM. She is also participating in the EU Research Project Emphasis, which deals with SCs. Her research interests include the modeling of supercapacitors, and she has experience both in modeling and software development and in laboratory practice, including signal generation, conditioning, and acquisition.

ORNELLA CONTI was born in Viterbo, Italy, in 2001. She received the bachelor's degree in electrical engineering from Politecnico di Torino, in 2023. She was with Politecnico to follow the ''path for enterprising students.'' She was involved in a long internship with INRIM, working on supercapacitor characterization and contributed to the extensive experimental testing of different devices, including model validation.

UMBERTO POGLIANO was born in Turin, Italy, in 1950. He received the Dr.Ing. degree in electronic engineering and the Ph.D. degree in metrology from Politecnico di Torino, in 1975 and 1987, respectively.

In 1977, he joined the Electrical Metrology Department, Istituto Nazionale di Ricerca Metrologica (INRIM), Turin, where his research focused on the development of systems and procedures for precise DC and AC low-frequency measurements. Since 2015, he has retired, but still cooperates as a Metrology Expert in some INRIM projects and activities. His research interests include AC-DC transfer standard, AC voltage, current, power measurements, generation, acquisition, and reconstruction of electrical signals.

• • •